HAL
open science

Multiple sulfur-isotope signatures in Archean sulfates and their implications for the chemistry and dynamics of the early atmosphere

Élodie Muller, Pascal P. Philippot, Claire Rollion-Bard, Pierre Cartigny

To cite this version:

Élodie Muller, Pascal P. Philippot, Claire Rollion-Bard, Pierre Cartigny. Multiple sulfur-isotope signatures in Archean sulfates and their implications for the chemistry and dynamics of the early atmosphere. Proceedings of the National Academy of Sciences of the United States of America, 2016, 113, pp.7432-7437. 10.1073/pnas.1520522113 . insu-01462972

HAL Id: insu-01462972

https://insu.hal.science/insu-01462972

Submitted on 22 Apr 2021

HAL is a multi-disciplinary open access archive for the deposit and dissemination of scientific research documents, whether they are published or not. The documents may come from teaching and research institutions in France or abroad, or from public or private research centers.

L'archive ouverte pluridisciplinaire **HAL**, est destinée au dépôt et à la diffusion de documents scientifiques de niveau recherche, publiés ou non, émanant des établissements d'enseignement et de recherche français ou étrangers, des laboratoires publics ou privés.

Multiple sulfur-isotope signatures in Archean sulfates and their implications for the chemistry and dynamics of the early atmosphere

Élodie Muller[a,1], Pascal Philippot[a,1], Claire Rollion-Bard[a], and Pierre Cartigny[a]

[a]Institut de Physique du Globe de Paris, Université Paris Diderot, Sorbonne Paris Cité, UMR 7154 CNRS, F-75238 Paris Cédex 05, France

Edited by Donald E. Canfield, Institute of Biology and Nordic Center for Earth Evolution (NordCEE), University of Southern Denmark, Odense M., Denmark, and approved May 17, 2016 (received for review October 16, 2015)

Sulfur isotopic anomalies ($\Delta^{33}S$ and $\Delta^{36}S$) have been used to trace the redox evolution of the Precambrian atmosphere and to document the photochemistry and transport properties of the modern atmosphere. Recently, it was shown that modern sulfate aerosols formed in an oxidizing atmosphere can display important isotopic anomalies, thus questioning the significance of Archean sulfate deposits. Here, we performed in situ 4S-isotope measurements of 3.2- and 3.5-billion-year (Ga)-old sulfates. This in situ approach allows us to investigate the diversity of Archean sulfate texture and mineralogy with unprecedented resolution and from then on to deconvolute the ocean and atmosphere Archean sulfur cycle. A striking feature of our data is a bimodal distribution of $\delta^{34}S$ values at ∼+5‰ and +9‰, which is matched by modern sulfate aerosols. The peak at +5‰ represents barite of different ages and host-rock lithology showing a wide range of $\Delta^{33}S$ between −1.77‰ and +0.24‰. These barites are interpreted as primary volcanic emissions formed by SO_2 photochemical processes with variable contribution of carbonyl sulfide (OCS) shielding in an evolving volcanic plume. The $\delta^{34}S$ peak at +9‰ is associated with non–^{33}S-anomalous barites displaying negative $\Delta^{36}S$ values, which are best interpreted as volcanic sulfate aerosols formed from OCS photolysis. Our findings confirm the occurrence of a volcanic photochemical pathway specific to the early reduced atmosphere but identify variability within the Archean sulfate isotope record that suggests persistence throughout Earth history of photochemical reactions characteristic of the present-day stratosphere.

Archean | sulfate | sulfur isotopes | atmosphere photochemistry

The amount of sulfate and its sulfur isotopic composition in the ocean through time is a function of the dynamic changes of sulfate sources (oxidative weathering on land, magmatic and hydrothermal input, and atmospheric photochemical reactions) and sulfate sinks (microbial and hydrothermal sulfate reduction and sulfate mineral precipitation). Although the Earth's sulfate budget can be reasonably well constrained after ∼2.3 billion years (Ga) ago, when free oxygen became a permanent component of the atmosphere, our understanding of the ocean sulfate budget before 2.3 Ga ago is subject to uncertainties. The occurrence of mass-independent sulfur-isotope anomalies (MIF-S, noted $\Delta^{33}S$ and $\Delta^{36}S$) in sedimentary sulfur (sulfide and sulfate) of Archean age (1) and the photochemical models (2) for the production and preservation of these anomalies support the view that the Archean atmospheric O_2 concentration was lower than 10^{-5} times the present atmospheric level. In this model, photochemical reactions involving volcanic SO_2 in the anoxic atmosphere yields both a reduced sulfur reservoir that can carry a highly positive $\Delta^{33}S$ and an oxidized sulfur reservoir with modestly negative $\Delta^{33}S$, the $\Delta^{36}S$ values being of opposite sign. The corollary to this model is that sulfate influx from oxidative weathering on land should have been low before ∼2.3 Ga ago. This assumption is supported by mass balance model of the Archean sulfur cycle, which showed that the total weathering flux of sulfur to the ocean was negligible before 2.8 Ga and about three to five times lower between 2.8 and 2.5 Ga compared with the Proterozoic (3). Known Archean sulfate deposits occur as barite ($BaSO_4$) associated with felsic volcanic rocks in Western Australia, India, and South Africa at about 3.5, 3.4, and 3.2 Ga (4). How sulfate appeared in the oceans during the early Archean when oxidative weathering was absent remains unresolved. Does it reflect a period of unique conditions for the preservation of sulfate, an exceptional period of intense sulfate aerosol production, or an unexpectedly active biological sulfur cycle?

Barite is one of the best proxy for investigating S- and O-isotope processes during the Precambrian (5). In contrast to pyrite or sulfate mineral such as anhydrite ($CaSO_4$), barite is poorly soluble and less prone to dissolution/recrystallization processes, so that the S and O isotopes can hardly be reequilibrated over geological time scales. Hence, a key issue for elucidating the early Archean sulfur cycle concerns the significance of the isotopic composition of Archean barites. The main deposits in Australia and South Africa define a narrow range of both $\delta^{34}S$ values between +3‰ and +8‰ and $\Delta^{33}S$ anomalies between −0.1‰ and −1.2‰ (1, 5–11). In contrast to the $\delta^{34}S$ values that are relatively constant in all barite deposits, the $\Delta^{33}S$ values define a potential trend increasing from 3.5 (∼−1.5‰) to 3.2 Ga (∼−0.5‰; Fig. S1) (10). The significance of these isotopic variations is subject of debate (Fig. S2). It has been attributed to mixing between a photochemical sulfate, with both negative $\Delta^{33}S$ and $\delta^{34}S$-values, representing the oxidized end product of a photochemical reaction that produced the so-called Archean reference array (ARA) of sulfides (possibly modified by bacterial processes), and an MDF sulfate (mass dependent fractionation,

Significance

In an anoxic world, sulfate is rare or absent and therefore unlikely to be preserved in the geological record. It is puzzling, therefore, that several sulfate deposits were formed during the Archean. In situ S-isotopic fingerprinting of Archean barite ($BaSO_4$) revealed that three main sources of photochemical sulfur were involved in their formation. A strongly negative $\Delta^{33}S$ possibly generated at the point of volcanic emission, a slightly positive $\Delta^{33}S$ overlapping modern stratosphere-piercing volcanic sulfate aerosols, and a ^{36}S-anomalous sulfate source matching carbonyl sulfide photolytic products now preserved as background atmospheric sulfate aerosols. It is suggested that Archean barite deposits represent an exceptional period of volcanic sulfate aerosol production and preservation rather than an unexpectedly active biological sulfur cycle.

Author contributions: P.P. designed research; E.M., P.P., C.R.-B., and P.C. performed research; C.R.-B. contributed new reagents/analytic tools; E.M., P.P., and C.R.-B. analyzed data; and E.M., P.P., C.R.-B., and P.C. wrote the paper.

The authors declare no conflict of interest.

This article is a PNAS Direct Submission.

[1]To whom correspondence may be addressed. Email: emuller@ipgp.fr or philippot@ipgp.fr.

This article contains supporting information online at www.pnas.org/lookup/suppl/doi:10.1073/pnas.1520522113/-/DCSupplemental.

Downloaded by guest on April 22, 2021

with $\Delta^{33,36}S = 0‰$) pool of mantellic origin modified either by microbial sulfide oxidation (10) or by disproportionation of magmatic/hydrothermal SO_2 in the ocean (7). Thus far, the two sulfate end members leading to MIF and MDF signals have not been found in the geological record. This model also fails to explain why barite was deposited during restricted periods of time between 3.5 and 3.2 Ga (4, 12). Based on the analysis of microscopic pyrites in felsic volcanic rocks displaying $\Delta^{33}S/\delta^{34}S$ relationships overlapping the isotopic composition of associated barite [Felsic volcanic array (FVA)], Philippot et al. (12) proposed that Archean barites could have formed temporally as volcanic ash deposits between 3.5 and 3.2 Ga ago (Fig. S2). In this model, most, if not all, sulfate may be of photochemical origin, with only minor overprint by MDF-sulfur processes. It also suggests that barite deposits should not be taken as representative of Archean oceans.

In situ analyses of Archean sedimentary sulfides with the secondary ion MS (SIMS) technique have revealed striking heterogeneities for $\delta^{34}S$, $\Delta^{33}S$, and $\Delta^{36}S$ at the grain and subgrain scales, which are not resolved by bulk SF_6 fluorination analyses (6, 12–14). Perhaps most importantly is that some in situ SIMS analyses yielded data in the four sulfur isotopes ($\delta^{34}S$, $\Delta^{33}S$, $\Delta^{36}S$) that cannot be identified by bulk analyses (14). In contrast to sulfide, Archean sulfate has never been investigated for its multiple sulfur-isotope composition using an in situ technique. Here, we present results of SIMS analyses of the four sulfur isotopes in early Archean barite and explore these data with the specific goal of examining the origin and significance of the relationship between $\delta^{34}S$, $\Delta^{33}S$, and $\Delta^{36}S$ to address the different sulfur sources and photochemical processes involved in their formation.

Geological Setting

The studied barites are from the 3.49-Ga-old Dresser Formation, Warrawoona Group (Pilbara Craton, Western Australia) and the 3.26- to 3.24-Ga-old Mapepe Formation of the Fig Tree Group (Barberton Greenstone Belt, South Africa). The barite deposit of the Dresser Formation consists of a succession of chert, barite, volcano-clastic sediments, hydrothermal breccia, and carbonates deposited in an active volcanic caldera (15, 16). This succession, also referred to as chert-barite unit, is overlain by pillowed basalts and underlain by spinifex-textured metabasalts that experienced low-grade metamorphism between 100 °C and 350 °C (16). The underlying komatiitic basalts occur transected by an extended network of meter- to kilometer-scale barite and black and white chert veins indicating intense hydrothermal circulations (15, 16). The bedded chert-barite unit varies between 4 and 60 m thick. It is composed of predominantly bedded chert and thick units of coarsely crystalline barite in layers sometimes several meters thick and oriented parallel, or discordant, to the bedding (Fig. S3 *A–C*). The barite deposits of the Mapepe Formation overlie unconformably the deep-water carbonaceous black cherts and komatiitic volcanic units at the top of the Mendon Formation (Onverwacht Group). They consist of millimeter-scale to tens of centimeter-thick beds of barite, which are hosted by a complex clastic and cherty sequence including spherule beds, thin chert layers locally ferruginous, a variety of greenish carbonated cherts representing silicified and carbonated felsic ash and containing disseminated barite locally evolving into barite beds (17), cherty sandstones containing detrital barite and jasper grains, and chert-pebble conglomerates (18) (Fig. S3 *D–J*). These lithologies indicate the deposition in a complex, volcanically active, coastal and fan-delta association (17) controlled by the emergence and erosion of tectonically unstable highs leading to rapid changes of lithology (18). The rocks of the Mapepe Formation experienced relatively minor deformation and low-grade metamorphism under lower greenschist facies (19), which resulted in the good preservation of the original sedimentary and diagenetic structures. A network of black and white chert veins and the occurrence of local barite impregnation in the komatiitic rocks of the Mendon Formation indicate the circulation of hydrothermal fluids during or soon after deposition.

The samples investigated were collected from the Barberton Barite Drilling Project (BBDP) drill core, which shows the transition from the Mendon Formation (Onverwacht Group) to the shallow water terrigeneous and volcanoclastic units of the Mapepe Formation, and from the Pilbara Drilling Project (PDP2b and PDP2c) drill cores, which intercepted the chert-barite unit of the Dresser Formation (16, 20). A subset of samples studied by Philippot et al. (6, 12) for pyrite analysis has been selected for barite analysis with the aim of evaluating the heterogeneities in the four sulfur isotopes at the grain and subgrain scales. Two types of barites were analyzed: bedded barites collected either as surface sample (Pi-06-23) of the Dresser Formation or at different depths of the BBDP (39.89, 76.76, 77.38, 78.10, and 78.18) and PDP (88.7a, 89.3a, and 96.6a) drill cores. With the exception of one sample (39.89), which represents a millimeter-scale layer of barite interleaved with felsic volcanic ash and chert (Fig. S3 *G* and *H*), all bedded barite samples correspond to thick layers of crystalline barite. These layers are generally composed of two main types of barite including (*i*) coarse-grained, sometimes sector- and oscillatory-zoned, barite blades, locally forming crystal fans and (*ii*) randomly oriented microcrystalline barite (Fig. S3 *B–F*). Eight samples of nonbedded sedimentary barites have also been selected in volcano-clastic sediments (45.12, 45.99, 56.66, 76.27, and 76.36), spherule beds (68.00 and 68.05), and cherts (50.25) of the BBDP drill core. These barites consist of micrometer-scale, randomly disseminated grains of likely terrigeneous origin (Fig. S3 *I* and *J*).

Results

Results for analyses are presented in Table S1. Bedded barite from both Dresser and Mapepe Formations shows two main types of S-isotope compositions. Type 1 displays $\delta^{34}S$ values between $+2.68 \pm 0.31‰$ and $+5.44 \pm 0.21‰$ and $\Delta^{33}S$ values between $-1.77 \pm 0.26‰$ and $+0.24 \pm 0.09‰$ (Fig. 1*A*). This type can be further subdivided into three main subtypes on the basis of their geological provenance and $\Delta^{33}S$ values. The lowest $\Delta^{33}S$ values between $-1.77 \pm 0.26‰$ and $-1.15 \pm 0.23‰$ ($\Delta^{33}S_{mean} \sim -1.41‰$) correspond to bedded barite from Dresser Formation. Barite with intermediate $\Delta^{33}S$ values between $-1.26 \pm 0.12‰$ and $-0.30 \pm 0.09‰$ ($\Delta^{33}S_{mean} \sim -0.98‰$) corresponds to meter-scale barite beds located at the base of the Mapepe Formation. The highest $\Delta^{33}S$ values between $-0.40 \pm 0.09‰$ and $+0.24 \pm 0.09‰$ ($\Delta^{33}S_{mean} \sim -0.10‰$) corresponds to a millimeter-scale barite layer of the Mapepe Formation interleaved within felsic volcanic ash and chert. Type 2 bedded barite shows higher $\delta^{34}S$ values between $+7.67 \pm 0.19‰$ and $+10.23 \pm 0.25‰$ and $\Delta^{33}S$ values between $-0.90 \pm 0.22‰$ and $-0.69 \pm 0.22‰$ for Dresser and $-0.56 \pm 0.10‰$ and $-0.02 \pm 0.10‰$ for Mapepe (Fig. 1*A*). This barite occurs in intimate association with type 1 bedded barite with low and intermediate $\Delta^{33}S$ values (Fig. S4). This relationship indicates that both types of barite deposited simultaneously during a same process. The preservation of grain-scale isotopic heterogeneities also suggests that the barite deposits represent primary precipitates, which were not subsequently rehomogenized in an open oceanic environment. Disseminated sedimentary barites present in terrigeneous volcano-clastic sediments, spherule beds, and laminated cherts of the Mapepe Formation show a range of $\delta^{34}S$ and $\Delta^{33}S$ values between $+4.08 \pm 0.28‰$ and $+11.00 \pm 0.39‰$, and $-1.03 \pm 0.09‰$ and $-0.18 \pm 0.22‰$, respectively (Fig. 1*C*). This range of composition is intermediate to the field defined by type 1 and type 2 bedded barites, which suggests that the disseminated barite have a mixed origin between these different sulfate sources. In a $\Delta^{33}S$-$\Delta^{36}S$ diagram, the different types of bedded barites show a different range of $\Delta^{36}S$ values (between $+0.67 \pm 0.51‰$ and $+2.12 \pm 0.24‰$ for type 1 with low $\Delta^{33}S$, $-1.37 \pm 0.54‰$ and $+1.92 \pm 0.29‰$ for type 1 with intermediate $\Delta^{33}S$, $-0.91 \pm 0.54‰$ and $+0.32 \pm 0.54‰$ for type 1 with high $\Delta^{33}S$, and $-1.58 \pm 0.54‰$ and $+1.68 \pm 0.42‰$ for

Downloaded by guest on April 22, 2021

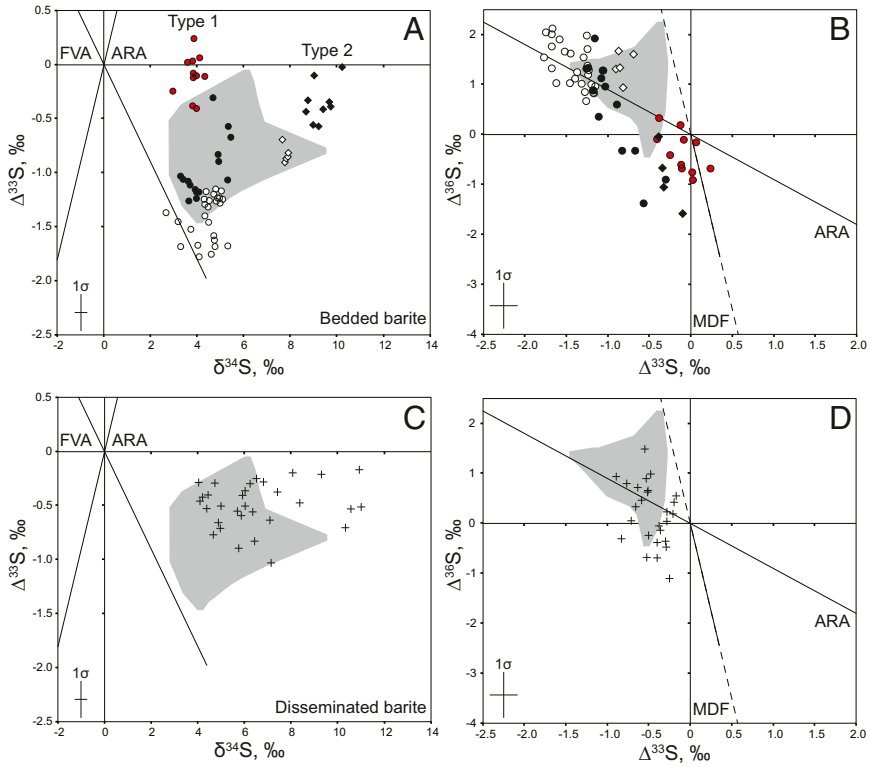

Fig. 1. In situ sulfur-isotope analyses of Archean sulfates. (*A* and *B*) Type 1 (circles) and type 2 (diamonds) bedded barites of the Dresser (open symbols) and Mapepe Formations (black symbols for meter-scale barite beds at the base of the Mapepe sedimentary sequence and red symbols for a millimeter-scale barite layer interleaved with felsic volcanic ash). (*C* and *D*) Disseminated barites of Mapepe Formation present in laminated chert, volcanoclastic sediment, and spherule bed (crosses). The 1σ error bars shown in *Inset* represent average uncertainties obtained on in situ sulfate analyses. The gray field represents the area defined by whole-rock analyses of Archean barite from the literature (1, 5–11, 49).

type 2; Fig. 1*B*). Taken individually, these different types define independent trends of steep slope centered on the ARA.

Discussion

A striking feature of our in situ barite analyses is a bimodal distribution of δ^{34}S values at about +5‰ and +9‰, which is matched by modern sulfate aerosols, but is not resolved by whole-barite analyses (single peak at +5‰; Fig. 2). This observation could be coincidental or indicates that Archean barite and modern sulfate aerosols have much in common (Fig. 3). Shaheen et al. (21) distinguished different sources of modern sulfate aerosols based on concentrations and δ^{34}S values of SO_4 in ice-core horizons. The low and intermediate δ^{34}S ranges (δ^{34}S = 1.4–2.6‰ and +12 ± 1.4‰) have been attributed to combining photoexcitation and photodissociation processes affecting different sulfur sources (mainly SO_2 and OCS) in the stratosphere. The most ^{34}S-enriched values correspond to seawater sulfate aerosols and to oxidation of organic compounds as DMS (δ^{34}S between +18‰ and +22‰). Accordingly, the two δ^{34}S peaks at ∼+5‰ and +9‰ (Fig. 2) suggest that similar SO_x photochemical processes were involved in the formation of Archean barite and modern stratospheric sulfate aerosols and that some of the isotopic differences (e.g., type 1 barite with different Δ^{33}S values; Figs. 1 and 3) could be explained by specific factors such as photolysis wavelength, gas pressure, and/or redox conditions.

The δ^{34}S peak at ∼+5‰ is defined by the different type 1 bedded barite of Dresser and Mapepe Formations (Fig. 1). Type 1 bedded barite with high Δ^{33}S values ($\Delta^{33}S_{mean}$ ∼−0.1‰ with a maximum value of +0.24 ± 0.09‰) is fully consistent with the range of modern stratospheric volcanic sulfate aerosols preserved in the ice and snow records (Fig. 3; δ^{34}S-Δ^{33}S slope ∼0.07 ± 0.01 and Δ^{33}S-Δ^{36}S slope ∼ −2.2 ± 0.4) (21–24), as well as laboratory experiments of SO_2 photodissociation in the 190- to 220-nm absorption region (δ^{34}S-Δ^{33}S slope = 0.086 ± 0.035 and Δ^{33}S-Δ^{36}S slope = −4.6 ± 1.3) (25, 26). This consistency between different sets of data, together with the observation that this type 1 barite is found in felsic volcanic ash, suggests that the same type of photolytic process, likely volcanic SO_2 photolysis, was effective both in the Archean atmosphere and modern stratosphere and potentially in the earliest Earth atmosphere (27). In contrast, type 1 barite with low and intermediate Δ^{33}S values is characteristic of Archean sulfate and was not identified in modern environments. Its origin is subject of debate. Previously identified by whole rock analyses, it has been attributed either to mixing between a photochemical sulfate with both negative Δ^{33}S and δ^{34}S values matching the ARA and a MDF seawater sulfate (7, 10) or to a photochemical sulfate reservoir of volcanic origin (FVA; Fig. S2) (12). Although our in situ analyses highlight the strong S-isotope heterogeneity of Archean barites (Fig. S4), no evidence of a photolytic sulfate pool matching the ARA could be identified in a δ^{34}S-Δ^{33}S space. The good overlap between the FVA and the most negative type 1 bedded barite of the Dresser Formation provides therefore support for a volcanic photolytic origin of these sulfates. We argue below that the Dresser barite reflects specific photochemical processes occurring at the point of volcanic emission.

Studies of sulfate aerosols in nature and in the laboratory have generally focused on homogeneous chemical reactions in the stratosphere, but ignored the initial chemistry and history of the volcanic plume because primary volcanic aerosols emitted at volcanic centers cannot be mass independently fractionated on modern Earth (28). However, owing to the absence of oxygen shielding short wavelength solar UV (<350 nm), it is likely that MIF production occurred at the source of volcanic emissions during the Archean. In present day volcanoes, sulfur gases represent typically 2–35%/vol of volcanic gas emissions (29). The dominant sulfur component is sulfur dioxide (SO_2) followed by hydrogen sulfide (H_2S). The SO_2 fraction increases with decreasing pressure (30) and with increasing temperature and oxygen concentration of the magma (29, 31). Carbonyl sulfide (OCS) and its precursor carbon disulfide (CS_2) contribute a small fraction of 10^{-4}% vol to 10^{-2}% vol. In contrast to SO_2, OCS has a residence time of several years in the atmosphere, and modern volcanoes are considered to contribute less than 1% to the total global atmospheric OCS emission (32). In an anoxic world, the contribution of OCS to the MIF-S budget may have

Downloaded by guest on April 22, 2021

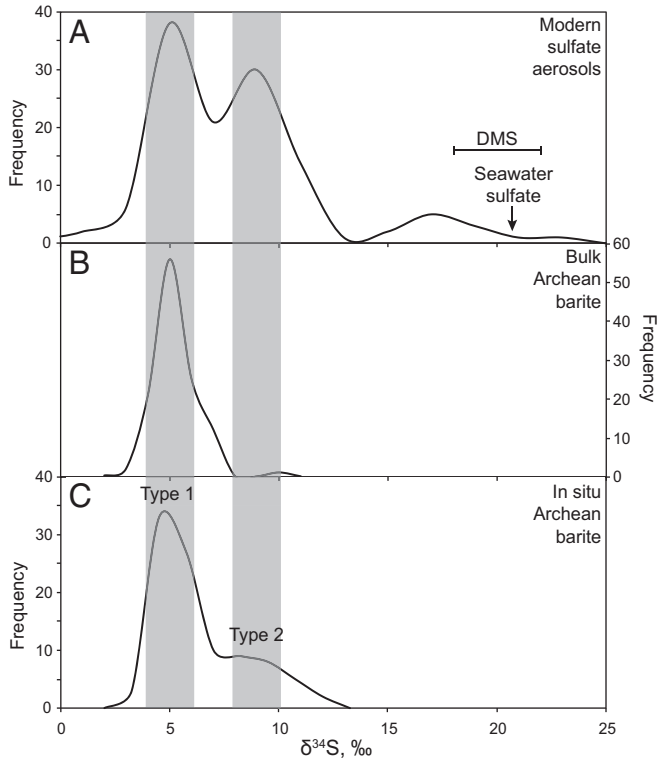

Fig. 2. Comparison of the frequency distribution of $\delta^{34}S$ composition in (*A*) present-day sulfate aerosols (n = 148, interval = 2‰) (21–24, 45, 50, 51) with (*B*) bulk (n = 140, interval = 1‰) 1, 5–11, 49), and (*C*) in situ (this study, n = 97, interval = 1.25‰) analyses of Archean barites. Modern and Archean sulfates define two main peaks at ∼+5‰ and +9‰ (highlighted in gray). The $\delta^{34}S$ of modern seawater sulfate (+21‰) and DMS (between +18‰ and +22‰) (52) are shown for comparison.

been much more significant than today. In reducing conditions, sulfur entering the atmosphere would be largely converted into OCS following the reaction $3CO + SO_2 = 2CO_2 + OCS$ (31). Ueno et al. (33) showed that high levels of carbonyl sulfide (OCS ∼ 1 ppm) would be expected if the plume is rich in CO (∼1%). In addition, previous studies of early planetary evolution predicted that OCS could be an important primary S volcanic species (34). Using a one-box model and considering a volcanic sulfur flux >3× larger than the modern volcanic outgassing rate (35), Ueno et al. (33) suggested that about 5 ppm of OCS is needed to explain the Archean $\Delta^{33}S$ record. The OCS molecule presents a large absorption cross section between 190 and 260 nm (36) and therefore has the ability to prevent SO_2 photolysis at UV wavelength greater than 202 nm. SO_2 photolysis between 180 and 200 nm produces sulfate with negative $\Delta^{33}S$ (33), which is typical of Archean barite. Accordingly, it is suggested that the sulfate source involved in the formation of type 1 barite could represent primary volcanic emissions formed by SO_2 photolysis with variable contribution of OCS shielding in an evolving volcanic plume (Fig. 4).

The $\Delta^{33}S$ variations recorded for Type 1 bedded barite of different ages (3.5 Ga old barite with low $\Delta^{33}S$ values, and 3.2 Ga old barite with intermediate and high $\Delta^{33}S$ values; Fig. S1) indicate that the $\Delta^{33}S$ of the photochemical sulfate products was not constant both in time and space. The most negative $\Delta^{33}S$ values associated with the massive bedded barite and vein network of the Dresser Formation could represent primary sulfate deposits formed at the point of volcanic emission where the density of SO_2 can increase by orders of magnitude in the days to weeks following a large eruption. This interpretation is supported by geological relationships indicating that Dresser barite formed in an active volcanic caldera (15, 16). Part of this SO_2 will react with CO to form OCS. OCS shielding combined with SO_2 shielding would in turn generate large amounts of sulfate and elemental sulfur aerosols with specific S-isotope characteristics, which would quantitatively overprint the isotope signal emerging from the background atmosphere. None of the broadband or single line SO_2 photochemical experiments available today can be used to account for the photochemical reactions occurring in dense volcanic plumes. Although displaying a negative slope subparallel to the FVA trend, SO_2 photolysis results using 193 nm UV (37) cannot be considered because of the extreme sensitivity of SO_2 isotopologue absorption cross-sections to UV wavelength (38). Accordingly, SO_2 photolysis experiments performed under various P-T-X conditions and integrating over the 180- to 202-nm UV range are needed to evaluate the photochemical significance of the FVA. In contrast, as discussed above, the high $\Delta^{33}S$ values ($\Delta^{33}S_{mean} \sim -0.1‰$) mimicking modern stratospheric sulfate aerosols may have formed at some distance from the point of emission through interaction with chemically and optically homogeneous volcanic plumes containing minor amounts of OCS. Intermediate ^{33}S-anomalous type 1 bedded barite of the Mapepe Formation ($\Delta^{33}S_{mean} \sim -1‰$) could represent mixing between these two end member sulfate sources.

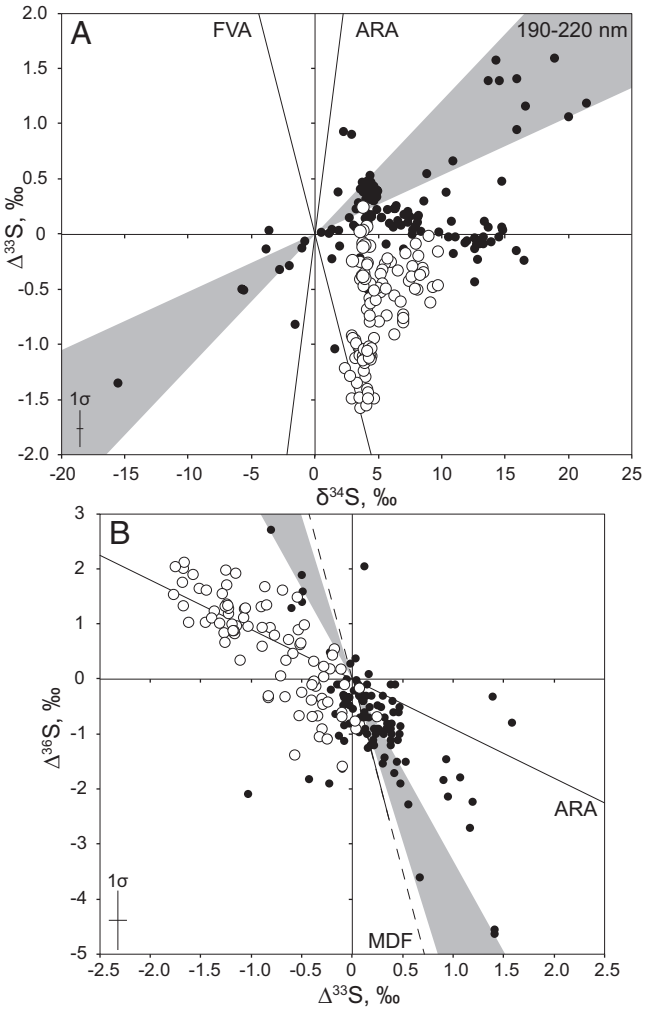

Fig. 3. Comparison of (*A*) $\delta^{34}S$-$\Delta^{33}S$ and (*B*) $\Delta^{33}S$-$\Delta^{36}S$ compositions of Archean bedded and disseminated barites from Dresser and Mapepe Formations (open circles; this study) with modern sulfate aerosols (black circles) (21–24, 50). The 1σ error bars shown in inset represent average uncertainties obtained on in situ analyses of sulfate. Gray field labeled 190–220 nm represents the experimental results of SO_2 photolysis using UV of wavelength 190–220 nm (Xe lamp) (25, 26).

Downloaded by guest on April 22, 2021

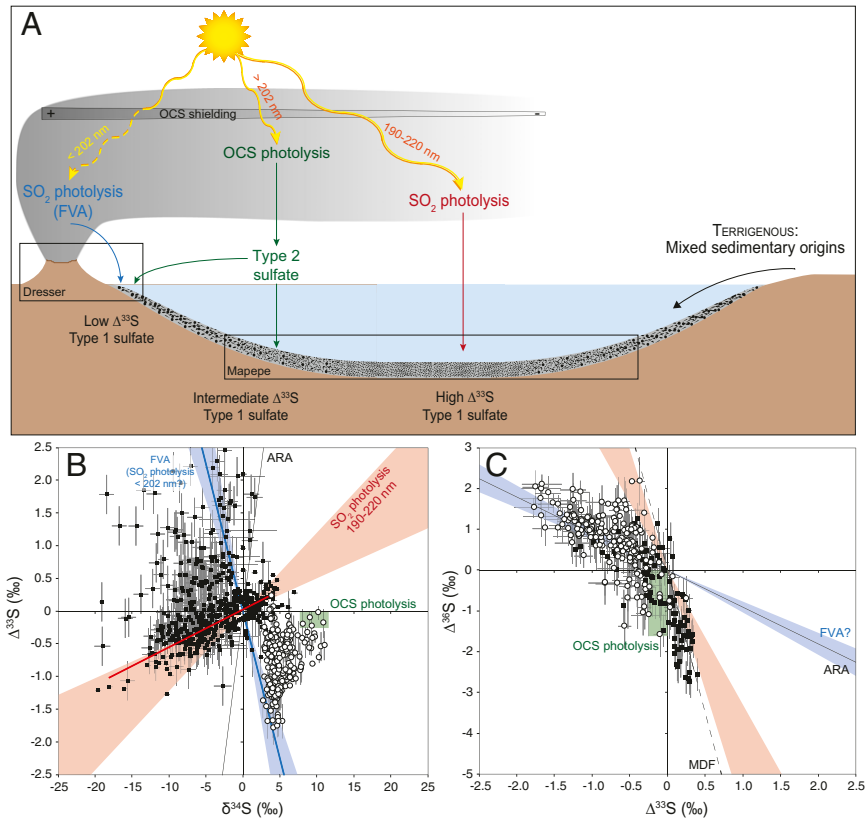

Fig. 4. Schematic model for the formation and deposition of Archean sulfate aerosols. (*A*) Different stages of volcanic activity and associated environments of barite deposition. (*B* and *C*) Sulfur isotopic compositions of barite (open circle; this study) (1, 5–11, 49) and sulfides (black square) (7–9, 49, 53) from Archean barite deposits and associated volcano-clastic and terrigenous sediments. Most of the sulfide isotopic compositions define a trend of slope 0.058 ± 0.003 (95% CI), similar to the experimental results of SO_2 photolysis using UV of wavelength of 190–220 nm (Xe lamp; red field) (25, 26). The green area represents the experimental results of OCS photolysis at $\lambda < 200$ nm (Xe lamp) (44). FVA (blue trend) is interpreted as OCS-shielded photolysis of SO_2 at $\lambda < 202$ nm.

The $\delta^{34}S$ peak at ~9‰ is defined by type 2 bedded barite of the Dresser and Mapepe Formations ($\Delta^{33}S$ up to 0‰; Fig. 1). The near-zero $\Delta^{33}S$ values could indicate a sulfate source of non-photochemical origin, such as the mantle, and the occurrence of positive $\delta^{34}S$ may highlight a MDF process, such as disproportionation of volcanic SO_2 (7) or microbial sulfate reduction (10). Hence, this ^{34}S-enriched sulfate reservoir may be representative of Archean seawater (7, 10). However, the negative $\Delta^{36}S$ values (−1.6 ± 0.5‰) recorded by the type 2 barite do not support these interpretations (Fig. 1) (39, 40). Shaheen et al. (21) reported anomalous sulfate aerosols with similar negative $\Delta^{36}S$ (−0.6 ± 0.2‰) formed either through OCS photolysis in the stratosphere or non-photochemical biomass and fossil fuel burning in the troposphere. Biomass and fossil fuel burning are unlikely for Archean environments. Hence, by a process of elimination, OCS photolysis remains the only process available to account for type 2 barite. On modern Earth, OCS is stored in the near surface of oceans and is released to the atmosphere through hydrolysis in seawater (41). The low solubility and long atmospheric lifetime with respect to tropospheric chemistry and photolysis enable a significant fraction of OCS to reach the stratosphere (42), where it photo-dissociates to carbon monoxide and elemental sulfur (S^0) on UV irradiation in the 200- to 260-nm range. The sulfur atom is oxidized by different pathways ($OH/H_2O_2/CO_2/O_3/O_2$) to SO_2 and ultimately sulfate, which is thought to contribute to the stratospheric sulfate aerosol layer (21, 43). Laboratory experiments have shown that OCS photolysis at short wavelengths does not produce ^{33}S-isotope anomaly in oxygen-free conditions but negative $\Delta^{36}S$ down to −1.5‰ (Fig. S5) (44). Accordingly, considering that OCS may have been an important sulfur component of the volcanic plume, it is suggested that sulfate aerosols could have formed through photolysis of OCS and oxidation of elemental sulfur by OH and/or H_2O_2 (45), the latter being efficiently generated in a CO_2/CH_4-rich and O_2-depleted Archean atmosphere (46). Direct photolysis and oxidation of OCS gases to sulfate aerosols on mineral and dust surfaces within the volcanic plume (47) could explain that both type 1 and type 2 barites coexist in a same sample (Fig. S4).

Conclusions

The presence of S-MIF in the present-day atmosphere in non-volcanic aerosols after the super ENSO 1997–1998 event has led Shaheen et al. (21) to suggest that both SO_2 and OCS sources could have contributed to sulfur-isotopic anomalies in the Archean. Our results fully support this hypothesis. In our model, however, considering the reducing nature of the early Earth, both SO_2 and OCS photolysis leading to elemental sulfur and sulfate aerosol production can occur during periods of active volcanism (Fig. 4). The origin of the strongly depleted ^{33}S-anomalies in Archean barites remains enigmatic. Our results tend to support the view of a photochemical process taking place near the point of volcanic emission. The recent findings by Roerdink et al. (48) that the different Archean barite deposits display different Sr-isotope ratios typical of the continental crust that are correlated with both ^{33}S-anomalies and barite age provide further support for a local (volcanic) rather than a global (marine) origin of Archean sulfate. If correct, this implies that Archean barites can be considered as important targets for studying the dynamics and atmosphere chemistry of early Earth but not earliest environments and emergence of microbial metabolisms. Because S isotopes of coexisting sulfate and sulfide involved in bacterial sulfate reduction and photochemical processes should

Downloaded by guest on April 22, 2021

follow specific trends, the feasibility of this claim could be tested in future studies by careful evaluation of sulfate and sulfide formation pathways and the existing geologic record.

Materials and Methods

In situ analyses of barite were performed with the CAMECA IMS 1280HR ion microprobe at Centre de Recherches Pétrographiques et Géochimiques (CRPG) with previously described procedures (12). The ion probe settings are basically the same for both the analysis of sulfides and sulfates (Table S2). Details of the analytical settings are described in *SI Materials and Methods* and in Fig. S6. The uncertainties (1σ) on $\delta^{34}S$, $\Delta^{33}S$, and $\Delta^{36}S$ are, respectively, around ±0.2‰, ±0.2‰, and ±0.5‰ on average.

ACKNOWLEDGMENTS. This work was supported by grants from the Programme National de Planétologie and the UnivEarths Labex Programme at Sorbonne Paris Cité (ANR-10-LABX-0023 and ANR-11-IDEX-0005-02). This is Institut de Physique du Globe de Paris contribution 3753.

1. Farquhar J, Bao H, Thiemens M (2000) Atmospheric influence of Earth's earliest sulfur cycle. *Science* 289(5480):756–759.
2. Pavlov AA, Kasting JF (2002) Mass-independent fractionation of sulfur isotopes in Archean sediments: Strong evidence for an anoxic Archean atmosphere. *Astrobiology* 2(1):27–41.
3. Stüeken EE, Catling DC, Buick R (2012) Contributions to late Archaean sulphur cycling by life on land. *Nat Geosci* 5(10):722–725.
4. Huston DL, Logan GA (2004) Barite, BIFs and bugs: Evidence for the evolution of the Earth's early hydrosphere. *Earth Planet Sci Lett* 220(1):41–55.
5. Bao H, Rumble D, III, Lowe DR (2007) The five stable isotope compositions of Fig Tree barites: Implications on sulfur cycle in ca. 3.2 Ga oceans. *Geochim Cosmochim Acta* 71(20):4868–4879.
6. Philippot P, et al. (2007) Early Archaean microorganisms preferred elemental sulfur, not sulfate. *Science* 317(5844):1534–1537.
7. Ueno Y, Ono S, Rumble DI, Maruyama S (2008) Quadruple sulfur isotope analysis of ca. 3.5 Ga Dresser Formation: New evidence for microbial sulfate reduction in the early Archean. *Geochim Cosmochim Acta* 72(23):5675–5691.
8. Shen Y, et al. (2009) Evaluating the role of microbial sulfate reduction in the early Archean using quadruple isotope systematics. *Earth Planet Sci Lett* 279(3):383–391.
9. Golding SD, et al. (2011) Earliest seafloor hydrothermal systems on Earth: Comparison with modern analogues. *Earliest Life on Earth: Habitats, Environments and Methods of Detection*, eds Golding SD, Glikson M (Springer Science + Business Media BV, Berlin), pp 15–49.
10. Roerdink DL, Mason PRD, Farquhar J, Reimer T (2012) Multiple sulfur isotopes in paleoarchean barites identify an important role for microbial sulfate reduction in the early marine environment. *Earth Planet Sci Lett* 331:177–186.
11. Montinaro A, et al. (2015) Paleoarchean sulfur cycling: Multiple sulfur isotope constraints from the Barberton Greenstone Belt, South Africa. *Precambrian Res* 267:311–322.
12. Philippot P, van Zuilen M, Rollion-Bard C (2012) Variations in atmospheric sulphur chemistry on early Earth linked to volcanic activity. *Nat Geosci* 5(9):668–674.
13. Mojzsis SJ, Coath CD, Greenwood JP, McKeegan KD, Harrison TM (2003) Mass-independent isotope effects in Archean (2.5 to 3.8 Ga) sedimentary sulfides determined by ion microprobe analysis. *Geochim Cosmochim Acta* 67:1635–1658.
14. Farquhar J, et al. (2013) Pathways for Neoarchean pyrite formation constrained by mass-independent sulfur isotopes. *Proc Natl Acad Sci USA* 110(44):17638–17643.
15. Nijman W, De Bruijne KCH, Valkering ME (1998) Growth fault control of Early Archaean cherts, barite mounds and chert-barite veins, North Pole Dome, eastern Pilbara, western Australia. *Precambrian Res* 88:25–52.
16. Van Kranendonk M, Philippot P, Lepot K, Bodorokos S, Pirajno F (2008) Geological setting of Earth's oldest fossils in the c. 3.5 Ga Dresser Formation, Pilbara Craton, western Australia. *Precambrian Res* 167:93–124.
17. Lowe DR, Nocita BW (1999) Foreland basin sedimentation in the Mapepe Formation, southern-facies Fig Tree Group. *Geologic Evolution of the Barberton Greenstone Belt, South Africa*, eds Lowe DR, Byerly GR (Geological Society of America, Boulder, CO), pp 233–258.
18. Heinrichs TK, Reimer TO (1977) A sedimentary barite deposit from the Archean Fig Tree Group of the Barberton Mountain Land (South Africa). *Econ Geol* 72:1426–1441.
19. Hofmann A (2005) The geochemistry of sedimentary rocks from the Fig Tree Group, Barberton greenstone belt: Implications for tectonic, hydrothermal and surface processes during mid-Archaean times. *Precambrian Res* 143:23–49.
20. Philippot P, et al. (2009) Early traces of life investigations in drilling Archean hydrothermal and sedimentary rocks of the Pilbara Craton, Western Australia and Barberton Greenstone Belt, South Africa. *C R Palevol* 8(7):649–663.
21. Shaheen R, et al. (2014) Large sulfur-isotope anomaly in nonvolcanic sulfate aerosol and its implications for the Archean atmosphere. *Proc Natl Acad Sci USA* 111(33): 11979–11983.
22. Savarino J, Romero A, Cole-Dai J, Bekki S, Thiemens MH (2003) UV induced mass-independent sulfur isotope fractionation in stratospheric volcanic sulfate. *Geophys Res Lett* 30(21):2131.
23. Baroni M, Thiemens MH, Delmas RJ, Savarino J (2007) Mass-independent sulfur isotopic compositions in stratospheric volcanic eruptions. *Science* 315(5808):84–87.
24. Baroni M, Savarino J, Cole-Dai J, Rai VK, Thiemens MH (2008) Anomalous sulfur isotope compositions of volcanic sulfate over the last millennium in Antarctic ice cores. *J Geophys Res* 113(D20):D20112.
25. Ono S, Whitehill AR, Lyons JR (2013) Contribution of isotopologue self-shielding to sulfur mass-independent fractionation during sulfur dioxide photolysis. *J Geophys Res* 118(5):2444–2454.
26. Whitehill AR, Jiang B, Guo H, Ono S (2015) SO_2 photolysis as a source for sulfur mass-independent isotope signatures in stratospheric aerosols. *Atmos Chem Phys* 15(4): 1843–1864.
27. Thomassot E, O'Neil J, Francis D, Cartigny P, Wing BA (2015) Atmospheric record in the Hadean Eon from multiple sulfur isotope measurements in Nuvvuagittuq Greenstone Belt (Nunavik, Quebec). *Proc Natl Acad Sci USA* 112(3):707–712.
28. Mather TA, et al. (2006) Oxygen and sulfur isotopic composition of volcanic sulfate aerosol at the point of emission. *J Geophys Res Atmos* 111(D18):D18205.
29. Textor C, Graf HF, Herzog M, Oberhuber JM (2003) Injection of gases into the stratosphere by explosive volcanic eruptions. *J Geophys Res Atmos* 108(D19):4606.
30. Gaillard F, Scaillet B, Arndt NT (2011) Atmospheric oxygenation caused by a change in volcanic degassing pressure. *Nature* 478(7368):229–232.
31. Oppenheimer C, Scaillet B, Martin RS (2011) Sulfur degassing from volcanoes: Source conditions, surveillance, plume chemistry and earth system impacts. *Rev Mineral Geochem* 73(1):363–421.
32. Andres RJ, Kasgnoc AD (1998) A time-averaged inventory of subaerial volcanic sulfur emissions. *J Geophys Res* 103(D19):25251–25261.
33. Ueno Y, et al. (2009) Geological sulfur isotopes indicate elevated OCS in the Archean atmosphere, solving faint young sun paradox. *Proc Natl Acad Sci USA* 106(35):14784–14789.
34. Fegley B (1991) Thermodynamic models of the chemistry of lunar volcanic gases. *Geophys Res Lett* 18(11):2073–2076.
35. Zahnle K, Claire M, Catling D (2006) The loss of mass-independent fractionation in sulfur due to a Palaeoproterozoic collapse of atmospheric methane. *Geobiology* 4(4): 271–283.
36. Molina LT, Lamb JJ, Molina MJ (1981) Temperature dependent UV absorption cross sections for carbonyl sulfide. *Geophys Res Lett* 8(9):1008–1011.
37. Farquhar J, Savarino J, Airieau S, Thiemens MH (2001) Observation of wavelength-sensitive mass-independent sulfur isotope effects during SO_2 photolysis: Implications for the early atmosphere. *J Geophys Res* 106(E12):32829–32839.
38. Claire MW, et al. (2014) Modeling the signature of sulfur mass-independent fractionation produced in the Archean atmosphere. *Geochim Cosmochim Acta* 141: 365–380.
39. Ono S, Wing B, Johnston D, Farquhar J, Rumble D (2006) Mass-dependent fractionation of quadruple stable sulfur isotope system as a new tracer of sulfur biogeochemical cycles. *Geochim Cosmochim Acta* 70(9):2238–2252.
40. Johnston DT, Farquhar J, Canfield DE (2007) Sulfur isotope insights into microbial sulfate reduction: When microbes meet models. *Geochim Cosmochim Acta* 71(16): 3929–3947.
41. Kettle AJ, Kuhn U, von Hobe M, Kesselmeier J, Andreae MO (2002) Global budget of atmospheric carbonyl sulphide: Temporal and spatial variations of the dominant sources and sinks. *J Geophys Res* 107(D22):4658.
42. Junge CE, Chagnon CW, Manson JE (1961) Stratospheric aerosols. *J Meteorol* 18: 81–108.
43. Brühl C, Lelieveld J, Crutzen PJ, Tost H (2012) The role of carbonyl sulphide as a source of stratospheric sulphate aerosol and its impact on climate. *Atmos Chem Phys* 12: 1239–1253.
44. Lin Y, Sim MS, Ono S (2011) Multiple-sulfur isotope effects during photolysis of carbonyl sulfide. *Atmos Chem Phys* 11:10283–10292.
45. Martin E, Bekki S, Ninin C, Bindeman I (2014) Volcanic sulfate aerosol formation in the troposphere. *J Geophys Res* 119(22):12660–12673.
46. Pecoits E, et al. (2015) Atmospheric hydrogen peroxide and Eoarchean iron formations. *Geobiology* 13(1):1–14.
47. Cwiertny DM, Young MA, Grassian VH (2008) Chemistry and photochemistry of mineral dust aerosol. *Annu Rev Phys Chem* 59:27–51.
48. Roerdink D, Hamelin C, Ronen Y, Mason P (2015) Sr isotopic insights into the formation of Paleoarchean barite. *Goldschmidt Abstracts* 2663. Available at goldschmidt.info/2015/abstracts/abstractView?abstractId=5067. Accessed June 6, 2016.
49. Hoering TC (1989) The isotopic composition of bedded barites from the Archean of southern India. *Geol Soc India* 34(5):461–466.
50. Romero AB, Thiemens MH (2003) Mass-independent sulfur isotopic compositions in present-day sulfate aerosols. *J Geophys Res Atmos* 108(D16):4524.
51. Bindeman IN, Eiler JM, Wing BA, Farquhar J (2007) Rare sulfur and triple oxygen isotope geochemistry of volcanogenic sulfate aerosols. *Geochim Cosmochim Acta* 71(9):2326–2343.
52. Watts SF (2000) The mass budgets of carbonyl sulfide, dimethyl sulfide, carbon disulfide and hydrogen sulfide. *Atmos Environ* 34:761–779.
53. Roerdink DL, Mason PR, Whitehouse MJ, Reimer T (2013) High-resolution quadruple sulfur isotope analyses of 3.2 Ga pyrite from the Barberton Greenstone Belt in South Africa reveal distinct environmental controls on sulfide isotopic arrays. *Geochim Cosmochim Acta* 117:203–215.
54. Whitehouse MJ (2013) Multiple sulfur isotope determination by SIMS: Evaluation of reference sulfides for $\Delta^{33}S$ with observations and a case study on the determination of $\Delta^{36}S$. *Geostand Geoanal Res* 37(1):19–33.

Downloaded by guest on April 22, 2021